Int. J. Electrochem. Sci., 17 **(2022)** Article Number: 22016, doi: 10.20964/2022.01.11

International Journal of
ELECTROCHEMICAL
SCIENCE
www.electrochemsci.org

Effect of Wide Ranges of Polarization and Concentration on the Behavior of Ferricyanide/Ferrocyanide Systems Studied Through Electrochemical Measurements

Moises Sanchez-Amaya[1], *Maximiliano Bárcena-Soto*[2], *René Antaño-López*[3], *Aaron Rodríguez-López*[4], *Jose Angel Barragan*[1], *Alberto Gutierrez-Becerra*[5], *Erika Roxana Larios-Durán*[1,*]

[1] Departamento de Ingeniería Química, Universidad de Guadalajara, C.P. 44430 Guadalajara, Jalisco, México
[2] Departamento de Química, Universidad de Guadalajara, C.P. 44430 Guadalajara, Jalisco, México
[3] Centro de Investigación y Desarrollo Tecnológico en Electroquímica, S. C., C.P. 76703 Pedro Escobedo, Querétaro, México
[4] Universidad Politécnica de Santa Rosa Jáuregui, C.P. 76220 Querétaro, Querétaro, México
[5] Departamento de Ciencias Básicas y Aplicadas, Universidad de Guadalajara, CUTonalá, C.P. 45452, Jalisco, México
[*]E-mail: erika.lduran@academicos.udg.mx

Received: 10 September 2021 / *Accepted:* 27 October 2021 / *Published:* 6 December 2021

The ferricyanide/ferrocyanide system has been historically utilized as an electrochemical standard under typical conditions, including dilute concentrations and narrow polarization ranges. Although deviations in the system's reversibility have been reported in broader experimental conditions, an electrochemical study that integrates the factors related to its idealities and nonidealities for an improved understanding of this redox couple has not been conducted. Therefore, in this paper, the electrochemical behavior of this system is investigated on a platinum electrode using 0.1 M K_2SO_4 as the supporting electrolyte under general experimental conditions at three $K_4[Fe(CN)_6]/K_3[Fe(CN)_6]$ concentrations (1 mM, 10 mM, and 0.1 M) and a widespread polarization potential range, which has not been conventionally reported. Through a literature review and the interpretation of cyclic voltammograms, double-layer capacitance polarization curves and electrochemical impedance spectra obtained under these conditions, a scheme of the global interfacial reactions involved in this system is proposed. As a result, a general approach to the mechanistic implications of the interfacial phenomena, including not only the reversible interfacial response but also the nonreversible behavior, is presented.

Keywords: Ferrocyanide/ferricyanide, Irreversibility of the system, Adsorbates on the electrode, Side reactions.

1. INTRODUCTION

Conventionally considered a reversible model system, the ferricyanide/ferrocyanide ($[Fe(CN)_6]^{3-}/[Fe(CN)_6]^{4-}$) couple is extensively applied as an electrochemical standard to assess surface charge transfer kinetics, allowing the characterization of interfacial processes and new electrode materials [1–6]. Shown in Eq. (1), this electrochemical reaction is often taken as a simple and fast one-electron transfer at the outer spheres of each complex [7–16].

$$[Fe(CN)_6]^{3-}{}_{(aq)} + e^- \leftrightharpoons [Fe(CN)_6]^{4-}{}_{(aq)} \quad (1)$$

In contrast, deviations in the system's reversibility have been attributed to the partial passivation of the electrode surface due to adsorbates, which entails mechanistic complications [1–3,5,17–26]. In this regard, secondary processes of this redox system have been evidenced using spectroscopic and electrochemical techniques that have generated a detailed characterization of the adsorbate nature, electrochemical response and impact on kinetics [1–3,5,8,9,12,17,21–29]. However, note that such investigations generally address these additional reactions on an individual basis. Thus, research conducted with more integrated perspectives should improve the phenomenological comprehension of this system.

Several studies indicate that ferrocyanide and ferricyanide chemisorbed on the electrode surface, as well as the products of their decompositions specified in Eqs. (2) and (3) [3,7,9,26,27,30–33]. Likewise, the generated free cyanide ion is well known to form a strong bond on the platinum electrode surface through its nitrogen [27,30], while the derived adsorbed iron ions may undergo redox reactions. Nevertheless, previous electrochemical works concerning these iron processes are scarce [18,34].

$$[Fe(CN)_6]^{3-}{}_{(ads)} \rightarrow Fe^{III}{}_{(ads)} + 6CN^-{}_{(ads)} \quad (2)$$

$$[Fe(CN)_6]^{4-}{}_{(ads)} \rightarrow Fe^{II}{}_{(ads)} + 6CN^-{}_{(ads)} \quad (3)$$

On the other hand, Prussian blue (PB) is recognized among the main adsorbates of the ferricyanide/ferrocyanide system [3,7,14,22,26,30,31,35–37]. PB is an attractive polymer that is highly investigated for its electrochromic properties and easy synthesis and that is commonly obtained in an acid solution (pH <4.0) that contains the supporting electrolyte and one or both species of the ferrocyanide/ferricyanide couple [34,38,39]. Low pH values are necessary for the decomposition of ferricyanide at feasible rates. The formation of colloidal PB ($KFe^{III}[Fe^{II}(CN)_6]_{(ads)}$, usually referred to as "soluble PB") is depicted in Eq. (4), which implies that the adsorbed iron ions coordinate with the adsorbed ferrocyanide and bind to the alkaline cation (K^+) of the electrolyte [38,40].

$$[Fe(CN)_6]^{4-}{}_{(ads)} + Fe^{III}{}_{(ads)} + K^+_{(aq)} \leftrightharpoons KFe^{III}[Fe^{II}(CN)_6]_{(ads)} \quad (4)$$

Furthermore, soluble PB can be reduced to Prussian white or can be oxidized to Berlin green, as shown in Eqs. (5) and (6) [34,41–43]:

$$KFe^{III}[Fe^{II}(CN)_6]_{(ads)} + K^+{}_{(aq)} + e^- \leftrightharpoons K_2Fe^{II}[Fe^{II}(CN)_6]_{(ads)} \quad (5)$$

$$Fe^{III}[Fe^{III}(CN)_6]_{(ads)} + K^+{}_{(aq)} + e^- \leftrightharpoons KFe^{III}[Fe^{II}(CN)_6]_{(ads)} \quad (6)$$

Many experimental conditions are alluded to benefit adsorbate formation at the electrochemical interface. High concentrations of the analyte, larger electrodes, repetitive and successive cycles of potential, extended potential ranges, long duration of the experimentation, overpotential values, composition of the supporting electrolyte, and longer prepolarization times in AC measurements, among others, can be cited [2,3,20,22,34,36,44].

Based on this background, the reversibility of the ferricyanide/ferrocyanide redox couple is achieved under specific conditions that may not be practical for various electrochemical studies. Hence, the results obtained under broader experimental conditions require a deeper interpretation from a mechanistic approach. This finding can be denoted in several publications, where the voltammetric response of ferricyanide/ferrocyanide at low concentrations and narrow polarization ranges is well known and considered reversible, while few cyclic voltammetries (CVs) performed in wider working ranges are reported to demonstrate its irreversibility associated with secondary reactions [8,34,44]. Therefore, general experimental studies that integrate not only reversible behavior but also irreversible behavior are desirable to understand the electrochemical response of the ferricyanide/ferrocyanide system.

Furthermore, the secondary processes of Eqs. (2)-(6) involve the presence of adsorbates on the electrode. These adsorption-desorption processes on the metallic surface can be addressed through double-layer capacitance (C_{dl}) measurements calculated from AC experiments [45–47]. The C_{dl} can be experimentally evaluated as a function of the polarization to determine the effect of the electrode charge on the selective adsorption of species. More importantly, typical C_{dl} curves allow us to identify the potential of zero charge (PZC), from which the determination of the favorable potential range for adsorption and interactions of each species is possible [45,48,49]. Since a minimal amount of information concerning the electrochemical double-layer response of ferricyanide/ferrocyanide has been reported [48], C_{dl} is an interesting aspect when studying the thermodynamic viability of the side reactions in Eqs. (2)-(6).

Additionally, electrochemical impedance spectroscopy (EIS) is a useful technique for identifying the different stages of an electrochemical reaction, whose sensitive response is expected to show anomalies of this redox system [50,51]. An adequate interpretation of EIS spectra requires the construction of relevant models with physical significance using either equivalent circuits and/or reaction mechanisms [50,52]. In a simplified manner for the former, a Randles circuit conventionally models the interface only considering the reversible redox reaction of ferricyanide/ferrocyanide in Eq. (1) [53,54]. Therefore, this circuit has been properly applied under certain experimental conditions, such as dilute concentrations and narrow frequency ranges. Since this model does not predict the experimental responses measured under more general conditions, other equivalent circuits should be analyzed to include anomalies related to adsorbates on the electrode surface [53]. Consequently, it is necessary to propose a general equivalent circuit that satisfactorily describes the global redox process of the ferricyanide/ferrocyanide system by incorporating the secondary reactions in more concentrated solutions and wider frequency ranges.

Therefore, the main objective of this work is to present a general study of the ferricyanide/ferrocyanide system and its behavior, including not only the reversible response but also the irreversible aspects related to secondary processes. This study is carried out on the basis of the exclusive use of routine electrochemical measurements, such as CVs, EIS and the response of C_{dl} as a function of the polarization potential, which are performed under broad experimental conditions using expanded polarization intervals and a wide concentration range of electroactive species. Accordingly, the redox couple concentration effect was investigated by performing measurements on a platinum electrode at three different concentrations of equimolar solutions of $K_4[Fe(CN)_6]/K_3[Fe(CN)_6]$ (1 mM,

10 mM, 0.1 M) in 0.1 M K_2SO_4 as the supporting electrolyte. This approach made it possible to demonstrate the sensitivity of these routine electrochemical techniques to determine the ideal response of the ferrocyanide/ferricyanide system and its deviations under broad experimental conditions. Furthermore, discussions about the mechanistic implications were analyzed on the basis of an extensive literature review and an integrated approach, allowing us to propose a novel global mechanistic scheme that can comprehend the interfacial reactions and species most likely involved in this system.

2. METHODS

2.1. Electrochemical cell

A conventional electrochemical cell kept at a controlled temperature of 22 °C (PolyScience MX7LR-20-A11B) and a water jacket were employed. A saturated calomel electrode (SCE) was selected as the reference electrode; a 1 cm diameter graphite rod was chosen as the counter electrode; and the working electrode was a platinum disc with a 0.79 cm^2 geometric area. When needed, the platinum electrode was cleaned by immersing it in concentrated HCl/HNO_3 (3 V:1 V), polished with alumina powder (50 μm) and rinsed copiously with distilled water. The working solutions consisted of 100 mL of equimolar amounts of $K_4[Fe(CN)_6] \cdot 3H_2O$ and $K_3[Fe(CN)_6]$ in 0.1 M K_2SO_4 as the supporting electrolyte. Accordingly, three different concentrations of the redox couple were prepared with distilled water: 1 mM, 10 mM and 0.1 M, whose pH ranged from 6-7. All reagents were analytical grade.

2.2. Measurements to evaluate the electrochemical response of the redox system

The electrochemical response of the ferricyanide/ferrocyanide system was analyzed by measurements of CVs, C_{dl} curves and EIS in freshly prepared working solutions. In all measurements, an AUTOLAB PGSTAT 128N potentiostat was employed.

To explore the effect of the polarization range, two sets of CVs were carried out, starting at open circuit potential, OCP (0.18, 0.19 and 0.21 V vs. SCE, for each working solution concentration, i.e., from the lowest to highest) toward positive potentials. First, five cycles of CVs were performed at a scanning rate of 10 mV/s in a regular potential window (i.e., η, $\pm$ 0.3 V vs. OCP) depending on each concentration to observe the typical and well-known reduction/oxidation peaks for the main reaction of Eq. (1) [1]. Second, CV experiments were carried out by significantly expanding the potential limits (i.e., η, $\pm$ 1.20 V vs. OCP) depending on each concentration to record at least 20 cycles at 20 mV/s. The literature suggests this scanning rate to decrease the duration of experimentation [3,34] and still attempts to visualize the electrochemical response from the interfacial processes of interest. Note that when the concentration of ferrocyanide and ferricyanide reaches the same concentration of the electrolyte, 0.1 M, the corresponding CVs are presented after ohmic drop correction, as described in a previous work [55].

Conventional EIS measurements were performed with a potential amplitude perturbation of 10 mV and seven points per logarithmic decade in the frequency range of 10 kHz - 1 mHz. For each concentration, EIS was determined at five overpotentials (η, V vs. OCP): 0 V, ± 0.03 V, which are

referred to as low-DC overpotentials (LDCO); and ± 0.20 V, which are referred to as high-DC-overpotentials (HDCO). To guarantee the steady state during the impedance measurement, chronoamperometries were previously performed by applying each mentioned overpotential for a variable time (600–1800 s), depending on the concentration and overpotential, until a stable current signal was obtained. When it was not possible to obtain a well-defined trend at the limit of the low frequencies, the unstable resulting EIS data were omitted. Proposed equivalent circuits were fitted to the EIS experimental data to calculate the theoretical electrical parameters through Zview® software. The validity and goodness of this procedure were evaluated through the statistical parameter χ^2, which reached an acceptable value of approximately $1x10^{-3}$ and revealed a good fit [56].

The C_{dl} curve was obtained from an AC experiment that is commonly named "AC voltammetry" or "impedance spectroscopy at a fixed frequency" [45,46]. The C_{dl} response was measured with a 10 mV amplitude, sinusoidal perturbation at a fixed frequency of 1 kHz for the lowest $K_4[Fe(CN)_6]/K_3[Fe(CN)_6]$ concentration, while 1 Hz was selected for the highest concentrations. The selected fixed frequency was chosen to ensure a capacitive response of the system. In all cases, the polarization potential was swept over an extended working range (i.e., η, $\pm$ 1.20 V vs. OCP) at a scan rate of 0.45 mV/s to guarantee a quasi-steady state response. The typical curve for C_{dl} vs. overpotential was computed from the imaginary component of these AC data.

2.3. Characterization of the interface modified by adsorbates

Further evidence apropos the adsorption processes was collected by immersing the working electrode in the three ferricyanide/ferrocyanide solutions and then applying different overpotentials (η, V vs. OCP) of 0 V or ±0.20 V for 1800 s. After each of these polarizations, the electrode was rinsed with distilled water and placed in pure supporting electrolyte, 0.1 M K_2SO_4 , to perform CVs at 10 mV/s. Consequently, any response different from the Pt voltammetric profile obtained in the blank solution of 0.1 M K_2SO_4 would presuppose the adsorption of ferricyanide/ferrocyanide ions from the working solution on the electrode. The voltammetric response of platinum in the pure background electrolyte, which was analyzed in a wide range of polarizations, would help elucidate any secondary processes solely related to the interactions of the platinum electrode and the background electrolyte [57] that may affect the analysis of the response of the ferrocyanide/ferricyanide couple and derived species.

3. RESULTS AND DISCUSSION

3.1. Cyclic voltammetry results of the ferricyanide/ferrocyanide system

This section presents the cyclic voltammograms of the platinum electrode from solutions of different concentrations of equimolar $K_4[Fe(CN)_6]/K_3[Fe(CN)_6]$ in 0.1 M K_2SO_4, where the current response I (mA/cm^2) is presented against the overpotential η (mV vs. OCP).

3.2.1 CVs with regular potential ranges

The results in Figure 1 are derived from applying a regular potential window that is suitable for each concentration. These typical voltammograms show the two well-expected peaks for this system, corresponding to the diffusion-controlled oxidation and reduction reactions of ferrocyanide and ferricyanide, respectively. Table 1 contains the reversibility criteria [58] calculated by the values for the separation of the anodic and cathodic peaks ΔEp and the ratio of the current redox peaks $|I_a/I_c|$ for each voltammogram. As observed, the values of $|I_a/I_c|$ decrease as the concentration of the redox couple increases, implying a lower concentration of ferrocyanide than ferricyanide, which is consistent with other publications [59,60]. In contrast, ΔEp increased with an increase in the concentration, far from the 59 mV ideal value for this system, denoting irreversibility [3,23]. These results should be expected since electrochemical reversibility is defined as plausible for small concentrations of the redox couple [58,61].

Other authors obtained similar results in relatively dilute solutions of this system [3,23,25,53], and their values of ΔEp expanded after successive cycles of potential or with a longer duration of experiments. They attributed this deviation to the formation of growing adsorbates that were partially blocking the electrode surface and slowing the electron transfer of Eq. (1) [3,17,25,53,62]. The same phenomenon could explain the results in Table 1, but unlike these results, here, the increment of ΔEp and the formation of adsorbates are associated with ion association, as evidenced by Eaton and other authors [25,59,60,63].

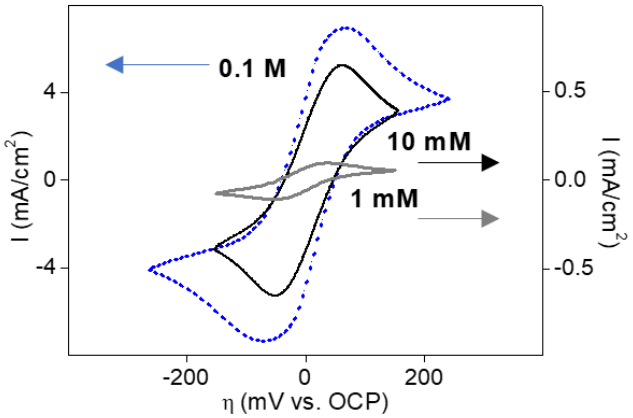

Figure 1. Typical cyclic voltammograms of a Pt electrode in solutions of different concentrations of equimolar $K_4[Fe(CN)_6]/K_3[Fe(CN)_6]$ in 0.1 M K_2SO_4 at the 2nd cycle with a scan rate of 10 mV/s. Ohmic drop correction is included for the highest $K_4[Fe(CN)_6]/K_3[Fe(CN)_6]$ concentration.

Table 1. Values of ΔEp and $|I_a/I_c|$ at different concentrations of equimolar $K_4[Fe(CN)_6]/K_3[Fe(CN)_6]$ in 0.1 M K_2SO_4.

Concentration	ΔEp (mV)	$\lvert I_a/I_c \rvert$
1 mM	71	1.08
10 mM	95	0.99
0.1 M	135	0.92

3.2.2 CVs with expanded potential windows

For a more complete exploration of the system, the potential limits were expanded in both anodic directions and cathodic directions, avoiding the reactions of water [3,34,38]. In this way, 20 successive cycles of CV were recorded at 20 mV/s starting from OCP toward positive values. The 2nd, 10th and 20th cycles are presented in Figure 2 for the three analyzed concentrations of the redox system. The 100th successive cycle is additionally shown in the upper left corner of each CV in Fig. 2.

In all cases, the oxidation/reduction processes of ferricyanide/ferrocyanide are observed by the clearly defined anodic peaks and cathodic peaks noticed in Figure 2 at overpotentials of approximately $+150$ mV and -150 mV vs. OCP, respectively. For the 1 mM and 10 mM solutions, the current response at negative overpotentials denotes a wide second cathodic peak ($\eta < -500$ mV) in addition to the typical peak of ferricyanide reduction. Likewise, for the highest concentration (0.1 M) in Figure 2c, crossovers in the current response are depicted ($\eta \sim -600$ mV) after a second cathodic peak ($\eta \sim -1000$ mV), which may imply a change on the electrode surface and allow us to correlate it to the deposition of metal [52]. Crossovers in the cathodic branch are related to nucleation and growth processes that suggest how the electrode surface has changed due to the presence of a metallic deposit on it [52].

Previous publications for this redox system have performed CVs with wider potential windows, generally expanding the working range only toward anodic potentials [34,38,44]; thus, the expanded cathodic responses of Figures 2a-c still have not been reported, and as a consequence, require a physical interpretation.

Among the species previously cited on the electrode surface, the adsorbed iron ions originated during the decomposition of ferrocyanide and ferricyanide in Eqs. (2) and (3) [27,30,62] may be involved in the unknown cathodic responses of Fig. 2. Accordingly, standard reduction potentials (V vs. SCE) for redox couples of $Fe^{3+}/Fe^{(0)}$, $Fe^{2+}/Fe^{(0)}$ and Fe^{3+}/Fe^{2+} are -0.28 V ($\eta\sim -470$ mV), -0.69 V ($\eta\sim -870$ mV) and $+0.53$ V ($\eta\sim +320$ mV), respectively [58], which suggests that for all the voltammograms in Fig. 2, the cathodic peak at high overpotentials and the crossovers observed at the highest concentration could be related to the deposition of iron. The deposition of iron has been described by a previously reported complex mechanism, which involves various stages and at least two adsorbed intermediates depending on the pH, supporting electrolyte and substrate [64]. However, for a qualitative general purpose, this process can be summarized as Eqs. (7) and (8)**.**

$$Fe^{III}{}_{(ads)} + e^- \leftrightharpoons Fe^{II}{}_{(ads)} \quad (7)$$

$$Fe^{II}{}_{(ads)} + 2e^- \leftrightharpoons Fe_{(s)} \quad (8)$$

Additionally, the redox reaction of Fe^{II}/Fe^{III} ions can be associated with a pair of small oxidation/reduction peaks at $\eta\sim +350$ mV, which are barely visible at the 20th cycle of Figure 2c but noticeable at the 100th cycle for the highest concentration analyzed.

Since the dissociations of ferricyanide and ferrocyanide provide the iron ion reactants of the reactions in Eqs. (7) and (8), both decompositions could be implicit in the results of Fig. 2. In this way, the voltammograms in Fig. 2a-c show how the ferricyanide reduction peak decreases after successive cycles of potential, which suggests its decomposition. Conversely, the dissociation of $[Fe(CN)_6]^{4-}$ can be inferred only at the 20th cycle for the highest concentration in Figure 2c, deduced from the smaller ferrocyanide oxidation peak. These results are consistent with previous spectroscopic works, where the

partial decomposition of ferricyanide has been observed notably more than that of ferrocyanide, since the latter is denoted by preferably maintaining its charge and structure [9,19,27,31,62]. This finding provides an explanation for the small presence of the peaks of the redox reaction of Fe^{II} to Fe^{III} ions at the 20th cycle of Figure 2c at $\eta\sim +350$ mV, since the decomposition of ferrocyanide is not as promoted as ferricyanide and the oxidation of Fe^{II} to Fe^{III} can be considered a slow process that may be more noticeable after 100 cycles. Additionally, it is observed that after 100 successive cycles of CV in the most concentrated solution, ferrocyanide and ferricyanide both decompose. Fig. 2c may also suggest that the adsorbed iron ions involved in Eqs. (7) and (8) might be the species more likely to remain at the interface at this point, which subsequently could lead to the covering of the electrode surface with iron deposit. The response shown at anodic overpotentials in Fig. 2c, upper left corner ($\eta\sim +350$ mV), is similar to a previous voltammetric response of the ferrous/ferric pair [65], reinforcing the abovementioned hypothesis. In agreement with this, similar responses to that observed in Fig. 2c, upper left corner, were obtained for the 100th cycle of CV in the other two concentrations (1 mM and 10 mM), as they showed the trend that was reached at the 20th cycle of each voltammogram. Our research team is working to gather additional experimental evidence in a future publication.

The current response at anodic overpotentials in Figure 2 was analyzed considering previous works. Similar to these studies, here, in addition to the ferrocyanide oxidation peak ($\eta\sim +150$ mV), it can be assumed that the PB redox reactions in Eq. (5) and Eq. (6) generate anodic peaks during CVs at approximately 0.17 V vs. SCE ($\eta\sim +150$ mV) and 0.84 V vs. SCE ($\eta\sim +750$ mV), respectively [34,42,44]. Thus, it is proposed that these peaks are superimposed on those related to ferrocyanide/ferricyanide charge transfer, since the electrochemical response of both electrochemical couples is reported to be very similar [34,42,44], as another study signified [3]. In contrast, the peaks for the PB/Berlin green redox reactions in Eq. (6) are visible high anodic overpotentials ($\eta\sim +750$ mV), which are evident for the lowest concentration in Figure 2a and are barely present at the 2nd cycle of Fig. 2b and 2c. Additionally, the PB/Berlin green redox peaks seem to decrease with successive cycles of potential. This finding is denoted in the lowest concentration voltammogram in Fig. 2a and becomes noticeable at the 10th and 20th cycles for the higher concentrations in Fig. 2b and 2c, where the peaks of PB/Berlin green are not observed. Similar irregularities in the Berlin green redox peaks have been published, reporting how their formation could not be corroborated during some PB electrochemical studies [38]. Based on these results, the pH of the working solutions applied in this work (6-7) appears to be an experimental condition that limits the formation of PB adsorbates in concentrated solutions. Nevertheless, previous works hinted that after "soluble PB" is formed on the surface under comparable pH conditions, it may leave the electrode and enter the bulk of the solution [3,35]. From another approach, the syntheses of PB in Eq. (4) generally state the dissociation of ferricyanide in Eq. (2) to be the key point since it provides ferric ions [3,34,66]. However, although the reaction in Eq. (2) was experimentally implicit in Figure 2, the redox responses for the PB adsorbates were notably low at higher concentrations. This finding could be presumably associated with the chemisorption of free CN^- ions [34], which are also produced by the reaction in Eq. (2). Thus, cyanide ions could occupy electroactive sites and block PB adsorption, as stated by previous studies [34,38]. In addition, the formation of PB polymers can additionally be impeded by the recoordination of free cyanides with ferric ions into $Fe(CN)_3$ or other products, as has been suggested in another work [34]. In accordance, reasonably for a

feasible electrodeposition of PB, most synthesis procedures state low pH values (<4) to benefit the formation of HCN and desorption of cyanides, resulting in more available electroactive sites [34,38].

In summary, the CVs in Figure 2 demonstrate the effect of the polarization potential range on the reversibility deviations and reveal how a wider polarization enhances side reactions that are not considered under regular polarization ranges. Thus, the following points can be highlighted: i) regardless of the electroactive ion concentration, successive cycles of potential and extended potential windows presumably promote the dissociation of ferrocyanide and ferricyanide, favoring the adsorption of their decomposition products. Moreover, the dissociation of ferricyanide was mainly promoted. ii) Adsorbed iron ions derived from these decompositions were attributed to redox reactions. iii) Cyanide ions could adsorb at the electrode and inhibit PB formation; and iv) a distinct redox response of the PB adsorbates was only evidenced at the lowest concentration. Even when these aspects are not noticeable in conventional studies that use narrower/regular potential ranges, the responses shown in Figure 2 describe a broader electrochemical behavior of the ferrocyanide/ferricyanide couple under more general experimental conditions.

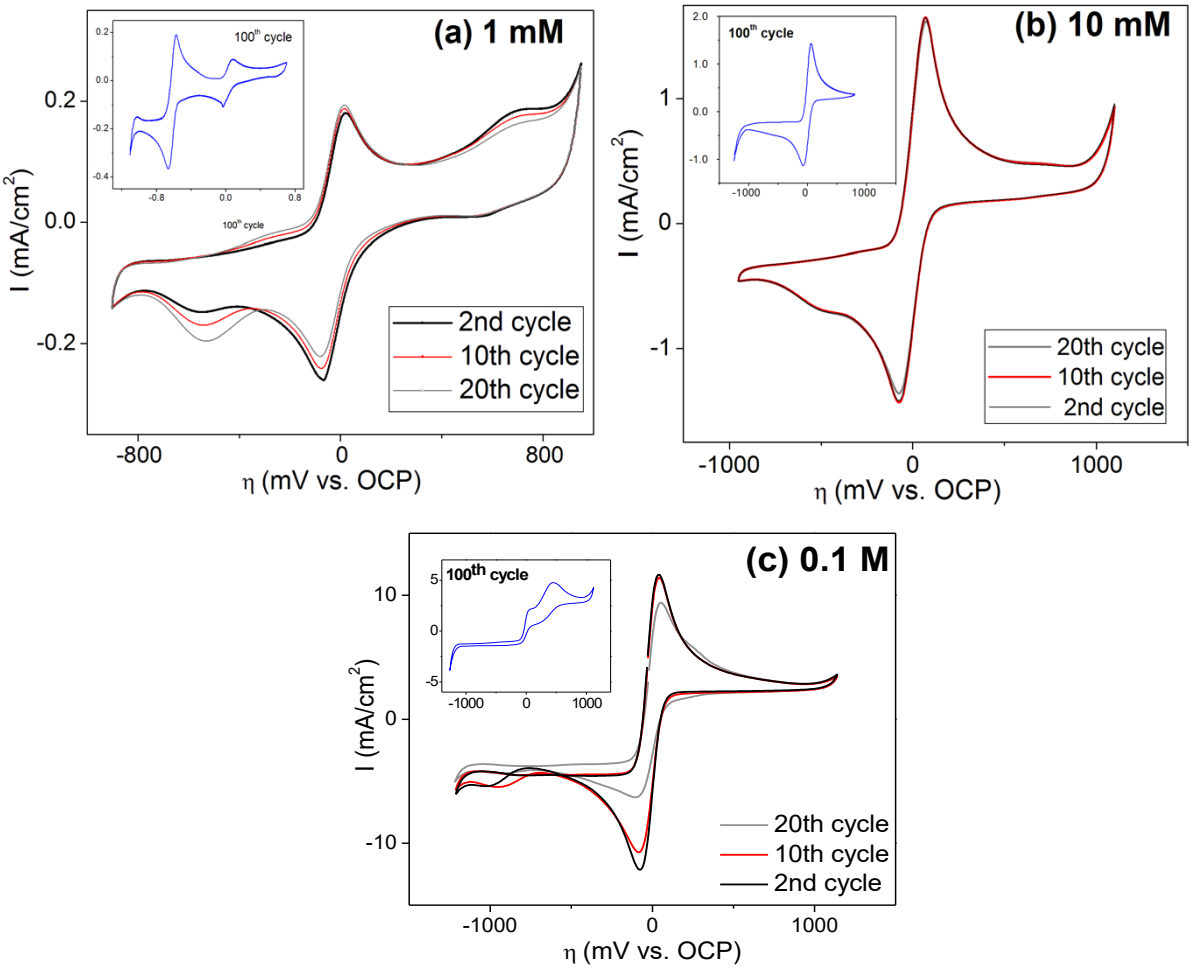

Figure 2. Cyclic voltammograms with expanded potential limits of a Pt electrode in solutions of different concentrations of equimolar $K_4[Fe(CN)_6]/K_3[Fe(CN)_6]$ in 0.1 M K_2SO_4 with a scan rate of 20 mV/s at the 2nd, 10th and 20th cycles. (a) 1 mM (b) 10 mM and (c) 0.1 M. Upper left corner in each CV refers at the 100th cycle. Ohmic drop correction is included for the highest $K_4[Fe(CN)_6]/K_3[Fe(CN)_6]$ concentration.

3.3. Voltammetric characterization of the adsorbates on the electrode

To evaluate the occurrence of spontaneous adsorption of ferricyanide/ferrocyanide ions and Eqs. (2)-(6), a clean working electrode was immersed in ferricyanide/ferrocyanide solutions for 1800 s at the OCP. In the same way, the effect of polarization on these adsorbates was investigated by applying two different overpotentials, ± 0.20 V vs. OCP, for 1800 s. After each of the aforementioned processes, the electrode was rinsed, and its voltammetric response was measured at 10 mV/s in pure 0.1 M K_2SO_4.

Figure 3 contains, as an example, typical CVs that include the pure platinum profile as the blank and the three different voltammetric responses of the electrode after immersion inside the most concentrated ferrocyanide/ferricyanide solution. The most notable difference among the Pt typical voltammetric profile [67] and the other CV responses can be pointed out as an additional cathodic *peak of interest* around $+150$ mV vs. SCE. No other responses, apart from the *peak of interest* and the Pt voltammetric profile obtained in the blank, are noticeable in the curves analyzed after polarizations at ± 0.20 V and 0 V vs. OCP. This *peak of interest* increases as the polarization becomes less negative, so it reaches a higher value of current in the following overpotential sequence: $+0.20\ \text{V} > 0\text{V/OCP} > -0.20\ \text{V}$. Similar tendencies in the voltammetric responses were observed at the other two analyzed concentrations (not shown), but the current magnitude decreased as the concentration of ferricyanide/ferrocyanide ions diminished, as expected.

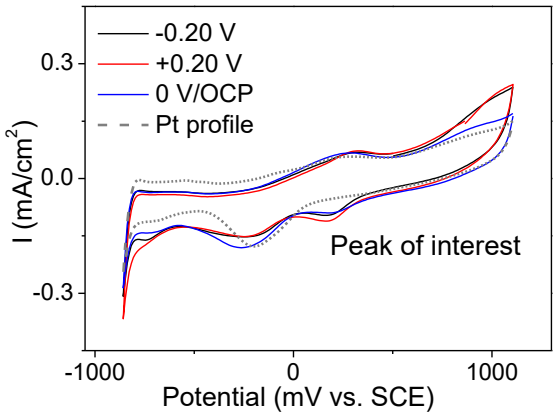

Figure 3. Cyclic voltammograms in pure 0.1 M K_2SO_4 at the 2nd cycle at 10 mV/s of a Pt electrode, which was previously rinsed after being modified by applying overpotentials (η, V vs. OCP) of 0 V/OCP and ± 0.20 V for 1800 s in 0.1 M equimolar $K_4[Fe(CN)_6]/K_3[Fe(CN)_6]$ in 0.1 M K_2SO_4.

According to the experimental conditions, the *peak of interest* observed in Figure 3 suggests that the adsorption of ferricyanide ions on the electrode is favored by the application of a selected overpotential, as previously exposed [20], and importantly, it may occur despite the absence of external polarizations at the OCP. This finding was explored in a previous literature report [3]. In that work, reversibility deviations in CVs were evidenced when the working electrode rested in a 10 mM redox couple concentration solution for 60 min at OCP. In this case, such deviations were associated with the adsorption of ions from the solution at the electrode surface. Furthermore, it could be inferred that since

the ferricyanide/ferrocyanide species adsorb at OCP, their following reactions are generated by the polarizations, i.e., Eqs. (4)-(6), could be plausibly considered parallel processes to the charge transfer in Eq. (1). This last statement suggests that the adsorption of the ions from the solution and PB formation could occur simultaneously with the main redox reaction [3,7], and furthermore, entails proposing a more general equivalent circuit that can describe the ferrocyanide/ferricyanide system when it is examined under more general conditions (refer to Section 3.5).

3.4. Dependence of the double-layer capacitance as a polarization potential function

Figure 4 shows as an example the schematic response of the double-layer capacitance C_{dl} against the overpotential, η (mV vs. OCP) for the most dilute concentration investigated. Similar responses were obtained for the other two concentrations analyzed (10 mM and 0.1 M). These results address the effect of polarization on the C_{dl} behavior and allow us to postulate the overpotential intervals where the adsorption and interactions between the adsorbates and the electrode are enhanced or inhibited [45]. Therefore, an electrostatic analysis of the adsorption of iron ions and CN^- is theoretically feasible through the C_{dl} curves.

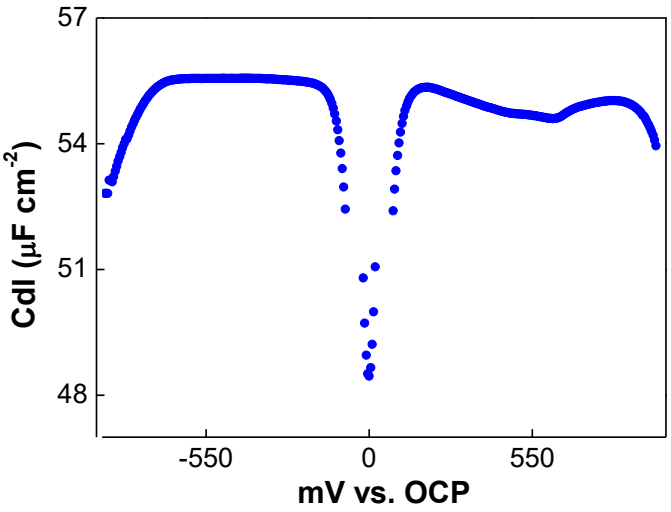

Figure 4. Double-layer capacitance curve as a function of overpotential with a scan rate of 0.45 mV/s obtained for a Pt electrode in 1 mM of equimolar $K_4[Fe(CN)_6]/K_3[Fe(CN)_6]$ in 0.1 M K_2SO_4 modulated at 1 kHz. C_{dl} was calculated from the imaginary part of these AC data.

Figure 4 exhibits a prominent minimum at the overpotential corresponding to 0 V (OCP). This minimum is located between two maxima ($-150 < \eta < +150$ mV) [45,68], which is consistent with a previous study in this redox system [48]. Based on the classical theory of double-layer capacitance, this minimum corresponds to the potential of zero charge (PZC) [45,68,69]. Thus, at more positive overpotentials than PZC, the adsorption of negative species such as ferrocyanide and ferricyanide is plausible regardless of the concentration of the redox couple. In addition, these adsorbed species might

subsequently decompose during polarization, as previously proposed. Once these decompositions take place, the adsorption of negative charges such as CN^- is also favored at more positive potentials than PZC. In an equivalent manner, the adsorption of positive charges, such as Fe^{III} and Fe^{II}, is favored at more negative potentials than PZC [68]. Thus, the C_{dl} curves could confirm the assumptions made in the previous sections related to cyanide adsorption at positive overpotentials inhibiting PB adsorption, as well as the occurrence of redox reactions of the adsorbed iron ions at negative overpotentials.

3.5. EIS results

This section presents the EIS spectra obtained for a platinum working electrode immersed in ferricyanide/ferrocyanide solutions at three different concentrations and at five overpotentials (η) previously specified as LDCO (OCP and ± 0.03 V) and HDCO (± 0.20 V). Figure 5 shows the complex-plane spectra in each experimental condition in an expanded limit of low frequencies, which is not usually presented in ferrocyanide/ferrocyanide studies. Here, the plots include a wide frequency range to expose a more complete response of the interface and evaluate not only its reversible behavior but also its possible deviations. In each spectrum, the experimental data are represented by symbols, while in some cases, the continuous lines indicate the fitting results when this procedure was possible.

The impedance responses measured at LDCO reveal that only for the lowest concentration evaluated in Fig. 5a does the impedance diagram show the typical expected response, revealing that the system behaves as an ideal, reversible, diffusion-controlled electron process in the investigated frequency range. This finding is evidenced by the presence of two time-constants observed at 1 mM, while at higher concentrations, in Fig. 5c and 5e, the number of time-constants increases, describing a more complex interfacial phenomenon evidenced by a second capacitive loop observed at the limit of low frequencies. From a mechanistic approach, complex-plane spectra exhibiting multiple time constants and/or multiple capacitive loops describe electrochemical systems with complicated faradaic processes [50,53], which include adsorption phenomena, coating formation/dissolution, and slow charge transfers, among others.

Similar impedance responses to those shown in Fig. 5e at $f < 10$ mHz have been previously reported [36,53]. In these works, the additional impedance response is attributed to the adsorption of species, such as ions from the solution, PB and/or the decomposition products of Eqs. (2) and (3) that form a coating on the surface. Based on the CVs shown in Figure 2, the presence of the additional impedance responses at LDCO could also be related to the redox reactions of the adsorbed iron ions shown in Eqs. (7) and (8), apart from the previously cited adsorption process [36,53]. In this manner, the impedance response suggests that the formation of this coating on the surface would be subsequent to the reaction in Eq. (1), as a previous study signified [53], occurring at low frequencies and being more noticeable in Fig. 5e for the more concentrated solution. Accordingly, the diameter of the low-frequency loop is smaller for the more negative polarization potential, where the deposition of iron coating would be more favorable. Likewise, for the case of the dilute solutions in Figs. 5a and 5c, the impedance responses for these consecutive reactions could not be accessible at these low overpotentials in the frequency range used during the experiments.

On the other hand, the spectra obtained at HDCO in Fig. 5b, 5d and 5f show a different response with a single capacitive loop over the whole frequency range and the absence of the diffusion-controlled charge transfer process, which is typical for this redox system.

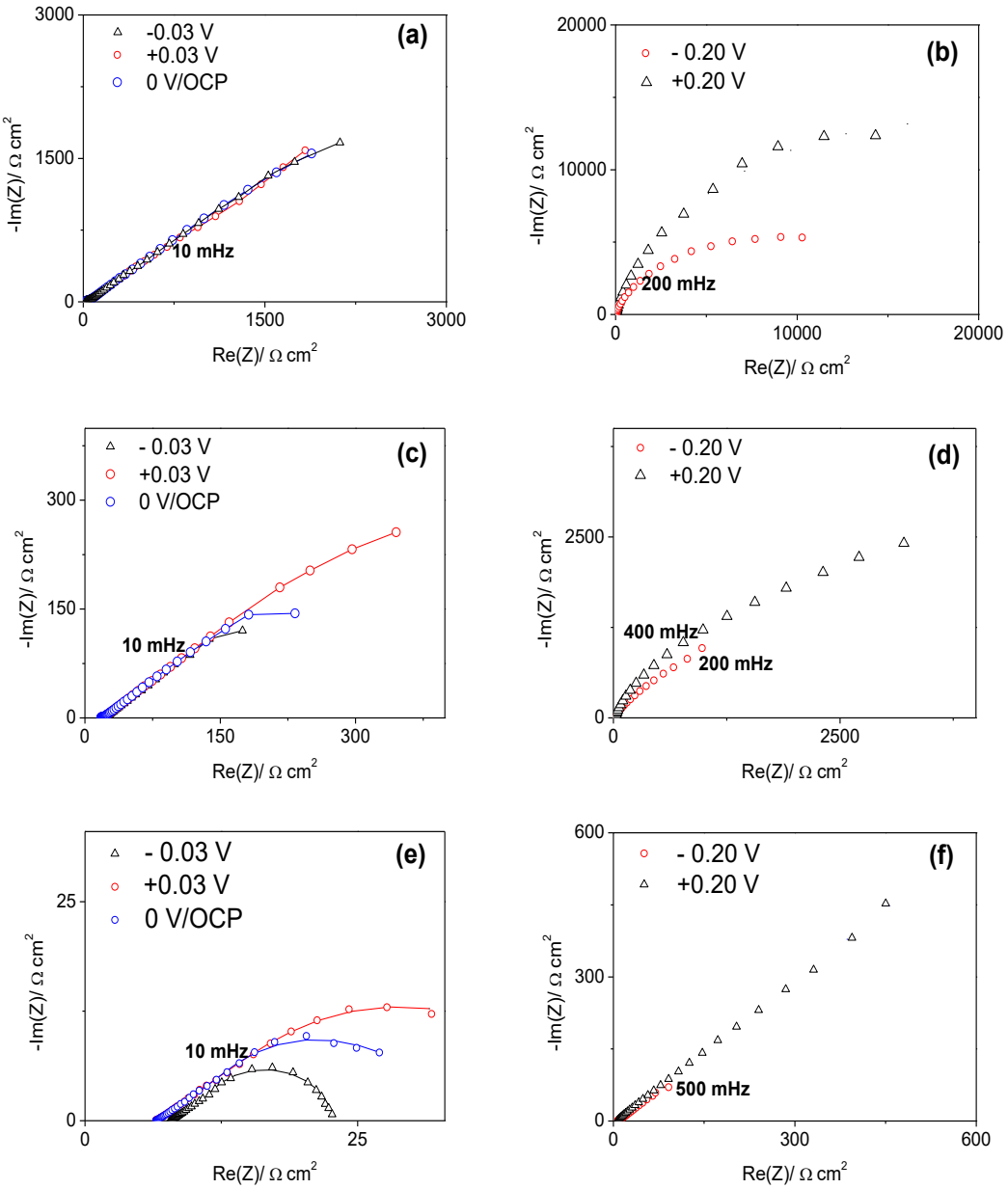

Figure 5. Complex-plane spectra for EIS on a platinum disc with a 10 mV potential amplitude perturbation for solutions of different concentrations of equimolar $K_4[Fe(CN)_6]/K_3[Fe(CN)_6]$ in 0.1 M K_2SO_4. (a) 1 mM LDCO, (b) 1 mM HDCO, (c) 10 mM LDCO, (d) 10 mM HDCO, (e) 0.1 M LDCO and (f) 0.1 M HDCO.

Moreover, regardless of the concentration, the impedance response reaches its highest values at $+0.20$ V, showing that at such overpotentials, the interface behaves much more resistive than at -0.20 V. These results suggest that at these high positive overpotentials, the interfacial reactions, such as those shown in Eqs. (1), (4)-(6), could be unfavored due to the presence of the CN^- adsorbates already proposed through the CVs and C_{dl} curves in the previous sections [53]. According to this finding, at

-0.20 V cyanide adsorption is not electrostatically favored, so the impedance values are lower and the faradic reactions for ferrocyanide/ferricyanide and adsorbed iron ions become more feasible.

3.6. Fitting EIS data through equivalent circuits

As previously mentioned, a Randles circuit is conventionally employed to fit the EIS data of the ferrocyanide/ferricyanide electrochemical system by only considering the main reaction of Eq. (1) [8,53,70] and could be used appropriately in dilute solutions, low overpotentials and limited frequency ranges. However, the Randles circuit does not predict the experimental data under more general experimental conditions. Therefore, an adequate equivalent circuit can be proposed to include the side reactions that affect the reversible EIS response of this system. A well-known variation of the Randles circuit is shown in Fig. 6a and consists of the electrolyte resistance Rs coupled in serial connection with a parallel arrangement of a nonideal, double-layer capacitance represented by a constant phase element CPE and the faradaic impedance of the ideal ferricyanide/ferrocyanide system, which is modeled by a serial combination of its charge transfer resistance Rct and a Warburg element W for its semiinfinite linear diffusion [53]. In another study, a modification of the previous Randles-like equivalent circuit was applied to describe the impedance response obtained for concentrations of $[Fe(CN)_6]^{4-}/[Fe(CN)_6]^{3-}$ above 25 mM [53]. In this arrangement, parallel resistance-capacitor coupling was added in serial connection with the Warburg element, assuming a consecutive reaction stage occurring after Eq. (1) at low frequencies. In that work, the authors assumed that this consecutive reaction stage described coating formation given by the chemisorption of ferrocyanide and ferricyanide, and their decomposition products shown in Eqs. (2) and (3) [53,54]. Nevertheless, as discussed in Sections 3.3 and 3.4, the spontaneous adsorption of ions from the solution at the OCP was feasible. In accordance, this result suggested that not only the processes in Eqs. (2) and (3) but also the formation of PB and its analogs described in Eqs. (4)-(6) can take place in parallel. Hence, the previously cited modified-Randles equivalent circuit can be improved by considering a parallel path for the side reactions connected to the Warburg element regardless of the concentration of the electroactive ion.

For the highest concentration solution, the formation of a metallic iron coating on the platinum electrode was suggested by the behavior observed at the expanded low frequency limit in the impedance spectra shown in Fig. 5e and the expanded cathodic limits of the CV shown in Fig. 2c. Therefore, the pathway nature of this step is suitable if modeled in serial to the main redox reaction of Eq. (1) and the side reactions established in Eqs. (2)-(6).

By the information collected thus far, two concentration-dependent circuits for a wide frequency range are proposed to fit the EIS data at LDCO, as shown in Figures 5a, 5c and 5e:

i) To account for the simultaneous processes observed at low frequencies and include the adsorption of ferricyanide/ferrocyanide and reactions in Eqs. (2)-(6), the resistance R_{HCF} was placed parallel to the faradaic impedance of the Randles-like circuit. Therefore, the arrangement shown in Fig. 6b was utilized to fit the EIS data of the 1 mM and 10 mM solution concentrations. The double-layer rearrangement related to all adsorbates is included in the nonideal capacitance CPE.

ii) For the most concentrated solution (0.1 M), the circuit shown in Fig. 6c was utilized. As observed, added serially to the usual Warburg element W and R_{HCF}, a parallel combination of a capacitor (C) and a resistor R_C that represents coating formation on the electrode was included.

Fitting the EIS experimental data of LDCO was performed through Zview® software taking into account a $\chi^2 \leq 10^{-3}$ as the goodness of fit. Thus, the capacitance C, the resistances *Rs*, *Rct*, R_{HCF}, R_C and the CPE parameters given by Eq. (9) are presented in Table 2, where a, b and c represent the concentrations of the main redox couple 1 mM, 10 mM and 0.1 M, respectively.

$$CPE = \frac{1}{Y_0(j\omega)^n} \quad (9)$$

In Eq. (11), ω is the frequency in $s^{-1,}$ and n ($0 \leq n \leq 1$) is a parameter related to the ideality of the double-layer capacitance.

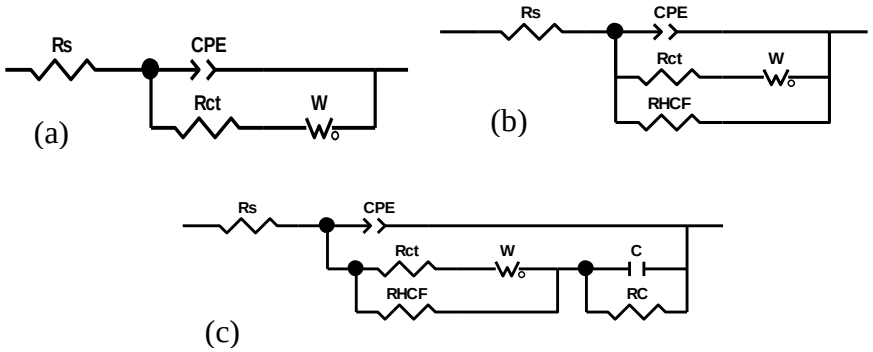

Figure 6. Implied equivalent circuits for fitting the EIS data at LDCO, depending on the concentration of equimolar $K_4[Fe(CN)_6]/K_3[Fe(CN)_6]$. (a) Conventional Randles arrangement, (b) proposed circuit for the 1 mM and 10 mM data and (c) proposed circuit for the 0.1 M data.

As observed in Table 2, the charge transfer resistance of the ferricyanide/ferrocyanide couple (Rct) decreases with higher concentrations, as expected. R_{HCF} has a smaller value at the positive overpotential, where the adsorption of ferrocyanide/ferricyanide and the reactions in Eqs. (2)-(6) were mentioned to be favored, in agreement with the previously presented C_{dl} curve presented. The relatively lower values of R_{HCF} at the 0.1 M solution suggests that the adsorption of ferricyanide/ferrocyanide and the reactions shown in Eqs. (2)-(6) are enhanced in concentrated solutions, which is in accordance with the discussion presented in Section 3.3. In the same manner, the high values of R_{HCF} for dilute solutions (1 mM) indicate that for low overpotentials ($\eta < \sim \pm 30$ mV vs. OCP) and small concentrations ($<$ 10 mM) the typical Randles circuit of Fig. 6a could be used to fit the EIS data, as expected. On the other hand, the resistance of the coating formation R_C reaches its higher value at the positive overpotential where metallic coating formation would not be favored.

Table 2. Fitted values of LDCO EIS data using the circuits from Figure 6, where *a*, *b* and *c* represent the concentrations of the main redox couple, 1 mM, 10 mM and 0.1 M, respectively.

η	*Rs*			*CPE*						*W*			*Rct*			R_{HCF}			R_C	*C*
	$\Omega\ cm^2$			$Yo\ X\ 10^4$ $(\Omega\ cm^2\ s^{-(1-n)})$			n			$\sigma\ X\ 10^3$ $(\Omega\ s^{-1/2} cm^{-1})$			$\Omega\ cm^2$			$k\Omega\ cm^2$		Ωcm	Ωcm^2	Fcm^{-2}
V vs. OCP	*a*	*b*	*c*	*a*	*b*	*c*	*a*	*b*	*c*	*a*	*b*	*c*	*a*	*b*	*c*	*a*	*b*	*c*	*c*	*c*
0	19	17	6	1.6	3.2	452.7	0.8	0.7	0.7	4	36	281	44	4	1	24	4	19	16	3.8
+0.03	21	17	6	1.6	2.4	243.3	0.8	0.7	0.7	3	21	221	50	4	1	18	3	8	18	5.0
-0.03	20	17	7	1.6	2.4	0.8	0.8	0.7	0.7	3	28	177	45	7	1	22	4	35	12	1.3

The Y_0 parameter of CPE has larger values for the more concentrated solution (0.1 M), suggesting how the interface could be deeply modified by the presence of a greater number of ions strongly adsorbed to the surface. This finding could be related to the presented voltammograms (refer to Fig. 2a) that evidenced the presence of the PB adsorbates only for the lowest concentration. The values of the capacitance C for the coating on the electrode surface are higher than the typical values of the double-layer capacitances reported in the literature for metallic electrodeposits [71–74].

Regarding the spectra obtained at high overpotentials (± 0.20 V) in Figures 5b, 5d and 5f, given that they do not present the typical response of the ferricyanide/ferrocyanide system, adjustment through equivalent circuits might not be feasible if it is conducted with a Randles-like circuit. Therefore, even when no equivalent circuit was fitted to the experimental impedance, they are presented for illustrative purposes to demonstrate the resistive response of the presence of adsorbates at high positive overpotentials.

3.7. General reaction mechanism scheme

The interfacial phenomena can now be expressed by the involved reactions and affected by the experimental conditions. Accordingly, and as a novel contribution, a reaction scheme, including the basic steps involved in this electrochemical system in the wider experimental conditions investigated in this work, is displayed in Figure 7. The first step **(I)** is the typical redox reaction for the ferrocyanide/ferricyanide couple, which is irreversible at high concentrations of the electroactive ion. Simultaneously, the dissociation of the adsorbed ferricyanide (**II)** and ferrocyanide **(III)** can develop. In addition, the adsorbed ferrocyanide and adsorbed ferric ions could coordinate with the potassium cation of the supporting electrolyte to obtain soluble PB**(IV).** Subsequently, soluble PB can be reduced to Prussian white **(V)** or oxidized to Berlin green **(VI)**. On the other hand, both adsorbed iron ions generated by dissociated ferrocyanide and ferricyanide could be oxidized to Fe^{III} or reduced to Fe^{II} ions, respectively **(VII)**. To conclude, the Fe^{II} ions may be further reduced to metallic iron **(VIII).**

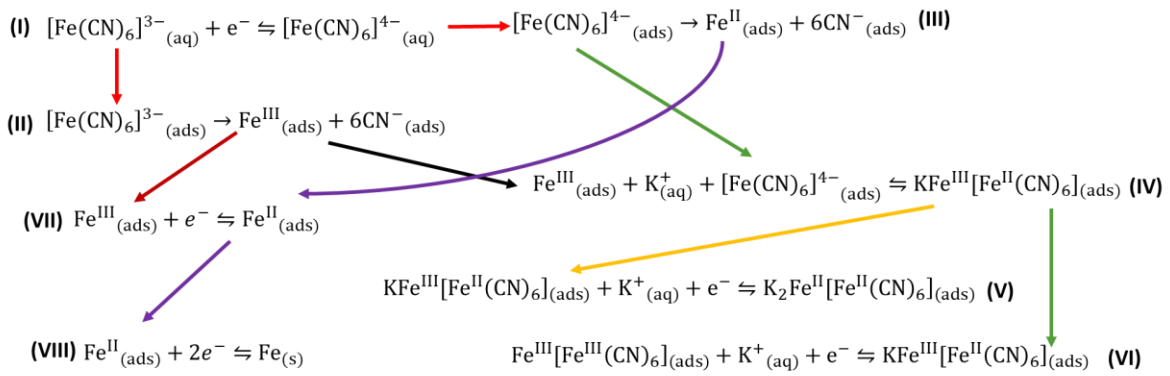

Figure 7. Proposed mechanistic scheme of the reactions involved at the electrochemical interface for the ferrocyanide/ferricyanide system under the experimental conditions of this work.

Therefore, it can be indicated that the presented scheme in Figure 7 can be summarized in the well-known reaction in **(I)** under typical experimental conditions. These typical conditions consider dilute concentrations of the redox couple (<10 mM), short duration of the experiments, regular potential windows (η< ~ ±150 mV vs. OCP) and limited frequency ranges (f>10 mHz). Based on previous studies, the mechanism here proposed could be still valid in other electrode materials, such as glassy carbon or gold electrode. This assumption is accepted as valid since in these electrodes, the electrochemical response reported also depicts secondary processes [36, 53, 75-76]

4. CONCLUSIONS

The ferricyanide/ferrocyanide system was investigated through CVs, C_{dl} curves and EIS measurements on a platinum disc electrode at three different concentrations (1 mM, 10 mM and 0.1 M) of equimolar $K_4[Fe(CN)_6]/K_3[Fe(CN)_6]$ in 0.1 M K_2SO_4 as the supporting electrolyte, in wide polarization intervals and frequency ranges expanded to low limits. According to the results obtained under these general experimental conditions, the reversibility of the redox couple system could be accurately approached at low concentrations (< ~10 mM) and small overpotential windows (η< ~ ±150 mV vs. OCP). At concentrated solutions and/or wider polarization ranges, different secondary processes could be evidenced by their electrochemical response. These additional reactions involve adsorbed species on the electrode and mainly include the formation of PB and the dissociation of ferrocyanide and ferricyanide on the electrode surface, producing iron ions that could undergo redox reactions.

ACKNOWLEDGEMENTS
MSA and JAB acknowledge the scholarships granted by CONACyT. The authors also thank CONACyT for the financial support to the project CF-2096004.

References

1. S.B. Emery, J.L. Hubbley, D. Roy, *Electrochim. Acta*, 50 (2005) 5659.
2. M. Risch, K.A. Stoerzinger, T.Z. Regier, D. Peak, S.Y. Sayed, Y. Shao-Horn, *J. Phys. Chem*. C, 119 (2015) 18903.
3. C.M. Pharr, P.R. Griffiths, *Anal. Chem*., 69 (1997) 4673.
4. D. Cai, X. Yang, B. Qu, T. Wang, *Chem. Commun*., 53 (2017) 6780.
5. C. Gabrielli, M. Keddam, N. Portail, P. Rousseau, H. Takenouti, V. Vivier, *J. Phys. Chem*. B, 110 (2006) 20478.
6. P. Iamprasertkun, A. Ejigu, R.A.W. Dryfe, *Chem. Sci*., 11 (2020) 6978.
7. A. Heras, A. Colina, V. Ruiz, J. López-Palacios, *Electroanalysis*, 15 (2003) 702.
8. L. Fernández Macía, M. Petrova, A. Hubin, *J. Electroanal. Chem*., 737 (2015) 46.
9. F. Kitamura, N. Nanbu, T. Ohsaka, K. Tokuda, *J. Electroanal. Chem*., 456 (1998) 113.
10. P. Boudeville, *Inorg. Chim. Acta*, 226 (1994) 69.
11. D.R. Rosseinsky, L. Glasser, H.D. Brooke Jenkins, *J. Am. Chem. Soc*., 126 (2004) 10472.
12. P.H. Daum, C.G. Enke, *Anal. Chem*., 41 (1969) 653.
13. V. Horvat-radošević, K. Kvastek, D. Križekar, *Croat. Chem. Acta*, 70 (1997) 537.
14. M.J. Hankins, G.S. Yablonsky, I.Z. Kiss, *PLoS One*, 12 (2017).
15. H. Gomathi, *Bull. Electrochem*., 16 (2000) 459.
16. S.A. Campbell, L.M. Peter, *J. Electroanal. Chem*., 364 (1994) 257.
17. S. Menolasina, *Rev. Téc. Ing. Univ. Zulia*., 28 (2005) 159.
18. S. Vogt, Q. Su, C. Gutiérrez-Sánchez, G. Nöll, *Anal. Chem*., 88 (2016) 4383.
19. V.N. Kiryushov, L.I. Skvortsova, T.P. Aleksandrova, *J. Anal. Chem*., 66 (2011) 510.
20. B.H. Loo, Y.G. Lee, E.J. Liang, W. Kiefer, *Chem. Phys. Lett*., 297 (1998) 83.
21. C. Beriet, D. Pletcher, *J. Electroanal. Chem*., 361 (1993) 93.
22. W. Huang, R. McCreery, *J. Electroanal. Chem*., 326 (1992).
23. K. Winkler, *J. Electroanal. Chem*., 388 (1995) 151.
24. X. Hua, H.L. Xia, Y.T. Long, *Chem. Sci*., 10 (2019) 6215.
25. M. Fleischmann, P.R. Graves, J. Robinson, *J. Electroanal. Chem*., 182 (1985) 87.
26. R. Noufi, D. Tench, L.F. Warren, *J. Electrochem. Soc. Electrochem. Sci. Technol*., 128 (1981) 2363.
27. K. Kunimatsu, K. Shigematsu, K. Uosaki, H. Kita, *J. Electroanal. Chem. Interfacial Electrochem*., 262 (1989) 195.
28. D.H. Angell, T. Dickinson, *Electroanal. Chem. Interfacial Chem*., 55 (1972) 55.
29. M.A. Sawhney, E.A. Azzopardi, S. Rodrigues Teixeira, L.W. Francis, R.S. Conlan, S.A. Gazze, *Electrochem. Commun*., 105 (2019) 106508.
30. K. Niwa, K. Doblhofer, *Electrochim. Acta*, 31 (1986) 439.
31. H. Baltruschat, F. Lu, D. Song, S.K. Lewis, D.C. Zapien, D.G. Frank, G.N. Salaita, A.T. Hubbard, *J. Electroanal. Chem*., 234 (1987) 229.
32. C. Korzeniewski, M.W. Severson, P.P. Schmidt, S. Pons, M. Fleischmann, *J. Phys. Chem*., 91 (1987) 5568.
33. S.J. Konopka, B. McDuffie, *Anal. Chem*., 42 (1970) 1741.
34. D. Zhang, K. Wang, D. Sun, X. Xia, H. Chen, *J. Solid State Electrochem*., 7 (2003) 561.
35. J. López-Palacios, A. Heras, Á. Colina, V. Ruiz, *Electrochim. Acta*, 49 (2004) 1027.
36. M. Sanchez-Amaya, M. Bárcena-Soto, A. Rodríguez-Lopez, R. Antaño-López, E.R. Larios-Durán, *Electrochem. Commun*., 117 (2020) 106769.
37. S. Husmann, E.S. Orth, A.J.G. Zarbin, *Electrochim. Acta*, 312 (2019) 380.
38. S. Husmann, A.J.G. Zarbin, R.A.W. Dryfe, *Electrochim. Acta*, 349 (2020) 136243.
39. R.K. Adhikamsetty, S.B. Jonnalagadda, *Bull. Chem. Soc. Ethiop*., 23 (2009) 47.
40. V. Plichon, S. Besbes, *Electrochim. Acta*, 37 (1992) 501.
41. K. Itaya, H. Akahoshi, S. Toshima, *J. Electrochem. Soc*., 129 (1982) 1498.

42. P. Najafisayar, M.E. Bahrololoom, *Thin Solid Films*, 542 (2013) 45.
43. J.J. García-Jareño, D. Benito, J. Navarro-Laboulais, F. Vicente, *J. Chem. Educ*., 75 (1998).
44. B.F. Baggio, C. Vicente, S. Pelegrini, C.C.P. Cid, I.S. Brandt, M.A. Tumelero, A.A. Pasa, *Materials* (Basel)., 12 (2019) 15.
45. B. Velasco-Rodriguez, J.F. Soltero-Martínez, L.C. Rosales-Rivera, E.R. Macías-Balleza, G. Landázuri, E.R. Larios-Durán, *ACS Omega*, 5 (2020) 17347.
46. M.A.V. Devanathan, B.V.K.S.R.A. Tilak, *Chem. Rev*., 65 (1965) 635.
47. T.R. Gore, T. Bond, W. Zhang, R.W.J. Scott, I.J. Burgess, *Electrochem. Commun*., 12 (2010) 1340.
48. R. Antaño-Lopez, Sur Une Nouvelle Methode de Caracterisation Des Processus Faradiques a Partir de Leur Couplage Avec La Capacite de La Double Couche (These de Doctorat), Université de Paris VI, 2001.
49. L.M. Bravo-Anaya, J.J. Gómez-Guzmán, F. Carvajal Ramos, R. Antaño-López, J.F.A. Soltero, E.R. Larios-Durán, *Electrochim. Acta*, 224 (2017) 142.
50. A. Lasia, Electrochem. Impedance Spectrosc. Its Appl., Springer (2014) New York, U.S.
51. M. Orazem, B. Tribollet, Electrochem. Impedance Spectrosc., I. John Wiley & Sons (2008) New Jersey, U.S.
52. I. Danaee, *J. Electroanal. Chem*., 662 (2011) 415.
53. S.H. Lee, H.Y. Fang, W.C. Chen, H.M. Lin, C.A. Chang, *Anal. Bioanal. Chem.*, 383 (2005) 532.
54. T.U. Noh, A.A. Aziz, *Chem. Eng. Trans*., 63 (2018) 529.
55. D. Garreau, J.M. Savéant, *J. Electroanal. Chem*., 35 (1972) 309.
56. A. Lasia, Electrochem. Impedance Spectrosc. Its Appl., Springer, (2014) New York, U.S.
57. U. Reimer, Y. Cai, R. Li, D. Froning, W. Lehnert, *J. Electrochem. Soc*., 166 (2019) F3098.
58. A.J. Bard, L. Faulkner, Electrochemical Methods. Fundamentals and Applications, John Wiley & Sons Inc., (1980) New York, U.S.
59. G.I. Hanania, D.H. Irvine, W.A. Eaton, P. George, *J. Phys. Chem*., 71 (1967) 2022.
60. W.A. Eaton, P. George, G.I. Hanania, *J. Phys. Chem*., 71 (1967) 2016.
61. T. Pajkossy, G. Mészáros, *J. Solid State Electrochem*., 24 (2020) 2883.
62. M. Stieble, K. Jüttner, *J. Electroanal. Chem*., 290 (1990) 163.
63. R.W. Chlebek, M.W. Lister, *Can. J. Chem*., 44 (1966) 437.
64. S.L. Díaz, J.A. Calderón, O.E. Barcia, O.R. Mattos, *Electrochim. Acta*, 53 (2008) 7426.
65. T. Ozeki, I. Watanabe, S. Ikeda, *J. Electroanal. Chem*., 236 (1987) 209.
66. S. Husmann, S.G. Booth, A.J.G. Zarbin, R.A.W. Dryfe, *J. Braz. Chem. Soc*., 29 (2018) 1130.
67. D. Chen, Q. Tao, L.W. Liao, S.X. Liu, Y.X. Chen, S. Ye, *Electrocatalysis*, 2 (2011) 207.
68. J.O. Bockris, A.K.N. Reddy, Modern Electrochemistry, Plenum Press, (1970) New York, U.S.
69. A.N. Frumkin, O.A. Petrii, B.B. Damaskin, Compr. Treatise Electrochem., Springer, (1980) New York, U.S.
70. D.A. Harrington, P. Van Den Driessche, *Electrochim. Acta*, 56 (2011) 8005.
71. S. Devaraj, N. Munichandraiah, *Electrochem. Solid-State Lett*., 8 (2005).
72. S. Yang, B. Deng, R. Ge, L. Zhang, H. Wang, Z. Zhang, W. Zhu, G. Wang, *Nanoscale Res. Lett*., 9 (2014).
73. J. Shi, X. Li, G. He, L. Zhang, M. Li, *J. Mater. Chem*. A, 3 (2015) 20619.
74. M. Del Grosso Destreri, J. Vogelsang, L. Fedrizzi, F. Deflorian, *Prog. Org. Coatings*, 37 (1999) 69
75. N. P. C. Stevens, M. B. Rooney, A. M. Bond and S. W. Feldberg, *J. Phys. Chem. A,* 105 (2001) 9087.
76. X. Hua, H. Xia and Y. Long, *Chem. Sci,* 10 (2019) 6215.